RESEARCH ARTICLE

Tunable single- and dual-wavelength lasers around 1.4 μm in Nd:LuGdAG crystal

Haotian Huang, Yuzhao Li, Nguyen Tuan Anh, Yanfei Lü, Jing Xia*

School of Physics and Astronomy, Yunnan University, Kunming, China

* xiajing_ynu@163.com

Abstract

We present the first diode-pumped tunable single- and dual-wavelength (DW) laser operation near 1.4 μm spectral region in Nd:LuGdAG (Nd:LGAG) crystal on the $^4F_{3/2} \rightarrow {}^4I_{13/2}$ transition. Three distinct lasing wavelengths at 1414 nm, 1426 nm and 1437 nm were generated by adjusting a Lyot filter (LF) in the cavity, respectively. The maximum continuous-wave (CW) power output of 3.64 W at 1414 nm was attained under an absorbed pump power of 18.7 W, exhibiting a slope efficiency of 23.7% and optical conversion efficiency of 19.5%. Further, three pairs of DW lasers operating at 1414 nm and 1426 nm, 1414 nm and 1437 nm, 1426 nm and 1437 nm were also achieved, respectively. The DW operation at 1414 nm and 1437 nm yielded 2.82 W total CW output power, attaining 15.1% total optical conversion efficiency. Single- and DW lasers in the 1410–1440 nm spectral range have important application in fields such as optical communication and medicine.

Citation: Huang H, Li Y, Anh NT, Lü Y, Xia J (2025) Tunable single- and dual-wavelength lasers around 1.4 μm in Nd:LuGdAG crystal. PLoS One 20(9): e0333387. https://doi.org/10.1371/journal.pone.0333387

Editor: Rajesh Sharma, Guru Ghasidas University Department of Pure & Applied Physics, INDIA

Received: May 16, 2025

Accepted: September 13, 2025

Published: September 26, 2025

Peer Review History: PLOS recognizes the benefits of transparency in the peer review process; therefore, we enable the publication of all of the content of peer review and author responses alongside final, published articles. The editorial history of this article is available here: https://doi.org/10.1371/journal.pone.0333387

1. Introduction

Nd-doped solid-state lasers predominantly employ three principal emission bands in the near-infrared spectrum: 0.9 μm corresponding to the three-level $^4F_{3/2} \rightarrow {}^4I_{9/2}$ transition, and four-level configurations at 1.1 μm ($^4F_{3/2} \rightarrow {}^4I_{11/2}$) and 1.3/1.4 μm ($^4F_{3/2} \rightarrow {}^4I_{13/2}$). Multiple Nd^{3+}-doped crystals including Nd:YVO_4 [1,2], Nd:YAG [3–5], Nd:$GdVO_4$ [6,7], Nd:YLF [8,9], Nd:YAP [10,11], Nd:CALGO [12] and Nd:GSAG [13–15] have demonstrated solid-state laser functionality. Conventionally, the 1.3 μm emission band in Nd-doped crystals originates from the $^4F_{3/2} \rightarrow {}^4I_{13/2}$ transition. However, this splitting phenomenon arises from the crystal field splitting effect, which partitions the energy levels into multiple Stark sublevels. Exemplified by Nd:YAG, such crystal fields induce over a dozen distinct emission peaks within the $^4F_{3/2} \rightarrow {}^4I_{13/2}$ manifold, with corresponding 1.4 μm region emissions having been documented in multiple studies [16–19]. Laser sources operating near 1.4 μm exhibit inherent eye-safe characteristics, enabling their deployment in diverse technical domains including optical communications, coherent LIDAR systems, dermatological treatments, advanced laser medicine, and ophthalmic therapies [20–25]. Among neodymium-doped laser

Data availability statement: All relevant data are within the manuscript.

Funding: This work has been supported by the National Natural Science Foundation of China (Grant Nos. 62175209 and 62241506).

Competing interests: The authors have declared that no competing interests exist.

crystals, Nd:LGYAG has been widely adopted in solid-state lasers due to its excellent optical quality and weak thermal lensing effect [26,27]. In the case of Nd:LGAG, Lu^{3+} and Gd^{3+} ions substitute for the totality of the Y^{3+} ions of the Nd:YAG but with a proportion $Lu^{3+}$and Gd^{3+} of about 30%. While The Nd:LGAG lasers at 1.1 [28], 0.9 [29] and 1.3 μm [30] have been implemented successfully in prior studies, systematic research on CW laser generation at 1.4 μm in the Nd:LGAG has not been reported until now. Fig 1 demonstrates the emission cross-section of the Nd:LGAG from 1250 nm to 1500 nm at room temperature on the $^4F_{3/2} \rightarrow {}^4I_{13/2}$ transition, which was calculated via the Füchtbauer-Ladenburg (F-L) formula [31]. It can be shown in Fig 1 that the strongest peak was 1332 nm. In addition, there were five peaks at 1316 nm, 1348 nm, 1414 nm, 1426 nm and 1437 nm.

In this study, we achieved three-wavelength tunability at 1414, 1426 and 1437 nm in Nd:LGAG on the $^4F_{3/2} \rightarrow {}^4I_{13/2}$ transition. Additionally, three pairs of DW tunability at 1414 nm and 1426 nm, 1414 nm and 1437 nm, 1426 nm and 1437 nm were also realized. Extensive implementation potential of DW laser systems has been identified across diverse technical domains including LIDAR systems [32], medical diagnostics [33], optical holography [34,35], precision spectral analysis [36], metrological sensing [37,38], nonlinear frequency conversion for UV/visible generation [39,40], and THz wave synthesis via difference frequency generation [41–43]. Especially, DW lasers around 1.4 μm enable simultaneous superficial epidermal heating and deep dermal collagen stimulation for non-invasive skin tightening and vascular coagulation, leveraging minimal thermal damage to surrounding tissues [44].

2. Experimental setup

The schematic diagram for the laser experiment was displayed in Fig 2. The pump system employs a 20 W 808 nm laser diode (LD) with a NA of 0.22 and a fiber core

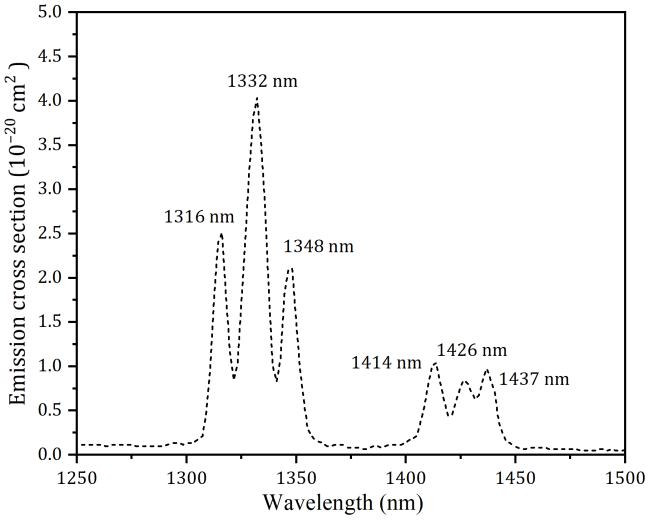

Fig 1. Emission spectrum of the Nd:LGAG in 1250 −1500 nm.

https://doi.org/10.1371/journal.pone.0333387.g001

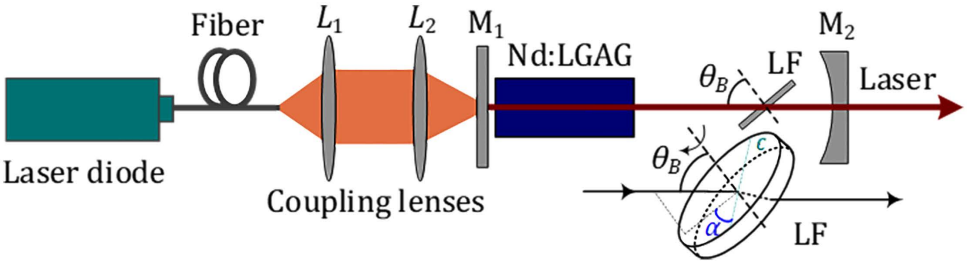

Fig 2. Schematic setup for the laser experiment. Inset: LF.

https://doi.org/10.1371/journal.pone.0333387.g002

diameter of 400μm. The radius of the pump spot was about 200 μm in the active medium. The laser spot radius in the active medium was about 190 μm. Two identical coupling lenses (L_1 and L_2) with a focal length of 100 mm were utilized, featuring anti-reflection (AR) at 808 nm on both surfaces. The measured transmittance of the optical coupling system exceeded 98%. A Nd:LGAG (1.0 at.% doping, 6 mm length) functioned as the active medium with AR at 808 nm and 1410-1440 nm, which was sealed in indium foil and affixed to red copper mounts equipped with water cooling, maintained at 15°C.

The cavity input coupler was a planar mirror (M_1) with AR for 808 nm and 1060–1350 nm, and high reflectivity (HR) at 1410–1440 nm. The cavity output coupler was a concave mirror (M_2) with a radius of curvature of –200 mm, a transmittance (T_{oc}) of 3.5% at 1410–1440 nm, and AR at 1060–1350 nm. Two other couplers (T_{oc} = 2.0% and 5.0%) were also carried out, with the M_2 demonstrated the optimal output performance. A quartz-based LF (4.0 mm thickness) was employed for wavelength tuning, positioned within the resonator at θ_B (Brewster angle) as depicted in Fig 2 inset. The tuning angle (α) was an angle between the optical axis of the LF (C) and the incident light projection on the LF surface.

3. Results and discussion

The single-pass transmittance for different wavelengths transmitted through the LF was expressed as [45]

$$T_{Lyot,i} = 1 - \frac{4cos^2\alpha sin^2\theta_B}{1-4cos^2\alpha cos^2\theta_B}\left(1 - \frac{cos^2\alpha sin^2\theta_B}{1-cos^2\alpha cos^2\theta_B}\right) sin^2\left(\frac{\delta_i}{2}\right), \quad (1)$$

where i = 1, 2 and 3 represents the 1414 nm, 1426 nm and 1437 nm three wavelengths, respectively, $\delta_i = 2\pi d(n_o - n_e)(1-\cos^2\alpha\cos^2\theta_B)/\lambda_i\sin\theta_B$ is an optical phase difference, n_o and n_e are the refractive indices of *o*- and *e*-light, respectively, d is a thickness of the filter. With Eq. (1) and the parameters: n_o = 1.5443, n_e = 1.5534, d = 4 mm and θ_B = 57.2°, the round-trip transmittance($T^2_{Lyot,i}$) of the different laser wavelength (λ_i) was calculated as a function of the tuning angle as displayed in Fig 3. It can be shown from Fig 3 that $T^2_{Lyot,i}$ can be controlled by regulating the LF surface around its normal axis. Thus, tuning between emission wavelengths can be realized by controlling the LF.

When tuning angle was rotated to about 38°, 39°, and 40°, the corresponding emissions at 1414 nm, 1426 nm, and 1437 nm were achieved, and their output-input performances were displayed in Fig 4. At an absorbed pump power of 18.7 W (corresponding to an incident power of 20 W) with T_{oc} = 3.5%, the laser demonstrated output powers of 3.64 W at 1414 nm, 3.01 W at 1426 nm, and 2.21 W at 1437 nm. The corresponding lasing thresholds were 2.70 W, 3.01 W and 3.21 W, with slope efficiencies of 23.7%, 19.4% and 14.5%, respectively. At T_{oc} = 2.0%, the laser demonstrated slope efficiencies of 18.3%, 15.2%, and 10.3% at 1414 nm, 1426 nm, and 1437 nm respectively, with corresponding threshold powers of 1.72 W, 2.12 W and 2.65 W. When T_{oc} was increased to 5.0%, the slope efficiencies changed to 17.4%, 14.6%, and 8.5%, while the threshold powers increased to 4.5 W, 5.7 W and 6.3 W for the respective wavelengths. The laser spectra

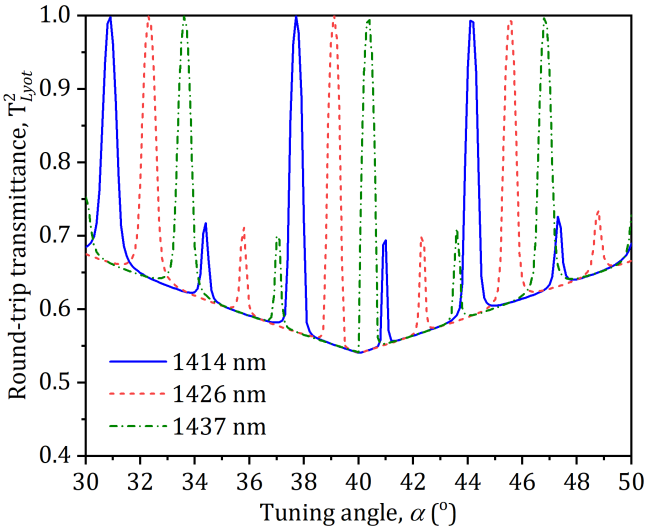

Fig 3. Round-trip transmittance (*T2 Lyot,i*) versus the tuning angle (α).

https://doi.org/10.1371/journal.pone.0333387.g003

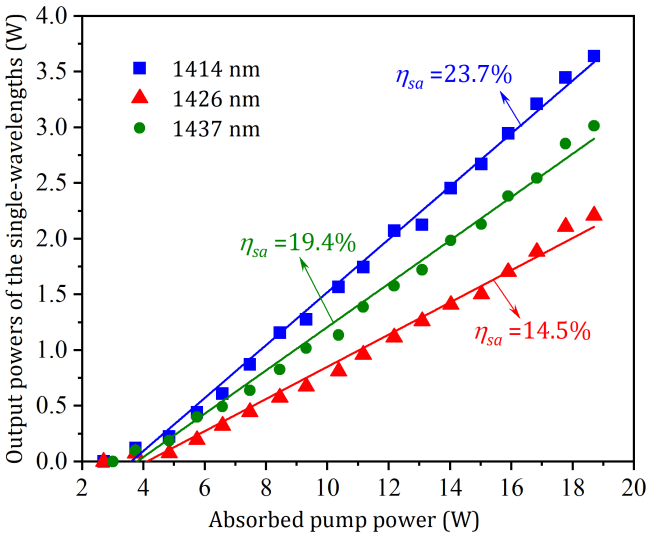

Fig 4. Output powers of the three single-wavelengths versus absorbed pump power.

https://doi.org/10.1371/journal.pone.0333387.g004

at 1414 nm, 1426 nm, and 1437 nm at the maximum pumping were displayed in the Fig 5. The corresponding wavelength peaks (1415.85 nm, 1426.28 nm and 1436.94 nm) exhibited spectral line width (FWHM) values of 0.30 nm, 0.33 nm and 0.35 nm, respectively.

The power stabilities of the three laser wavelengths were measured with a precision power meter. The power fluctuations (RMS) at the maximum output powers were about 2.7%, 3.6% and 3.9% in 1 hour, respectively, as shown in Fig 6. The insets (a)-(c) of Fig 6 show the measured radii and the beam quality factors (M^2) of the 1414 nm, 1426 nm, and 1437 nm beams, respectively. The beam quality factors (M^2) of the 1414 nm, 1426 nm, and 1437 nm wavelengths were

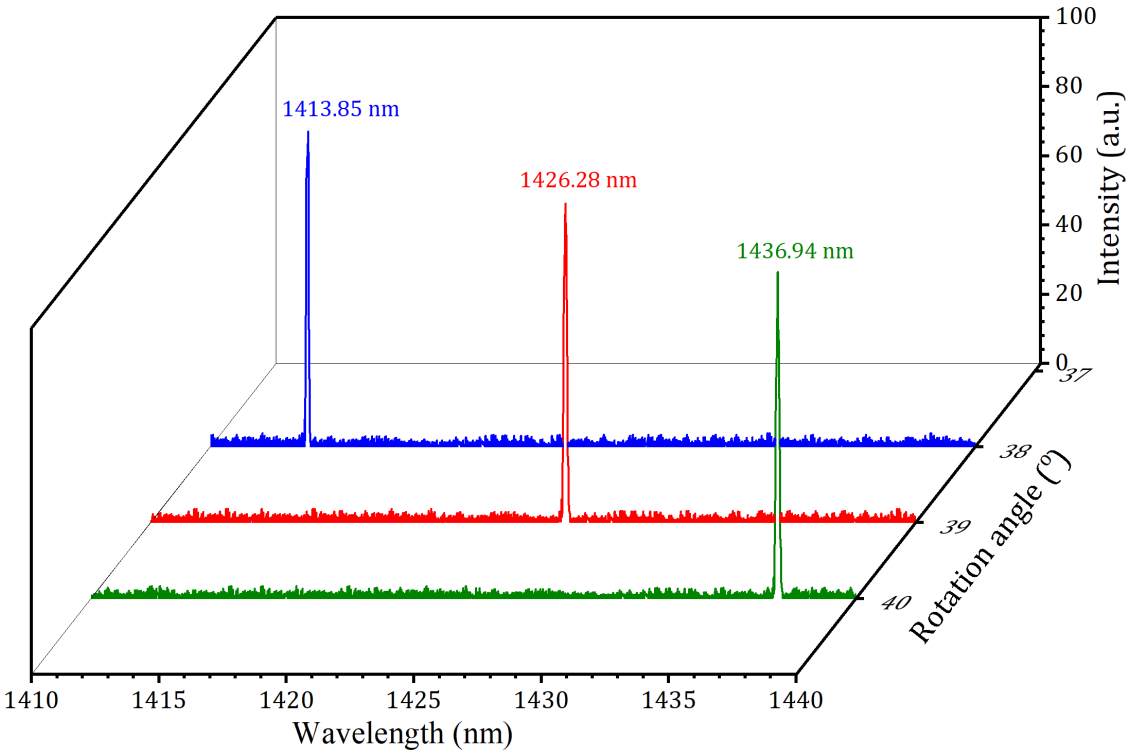

Fig 5. Laser spectra of the three single-wavelengths.

https://doi.org/10.1371/journal.pone.0333387.g005

measured using the knife-edge technique. The corresponding values in both transverse directions at maximum output power were less than 1.16, 1.12 and 1.25, respectively.

For a four-level laser system operating with CW, the oscillation threshold of each emission wavelength in a DW operation was given by [46]

$$P_{tha,i} = \frac{-ln\left(1 - T_{oc}\right) + L_i + L_{0i}}{2l_c\eta_{q,i}} \frac{h\nu_p}{\sigma_i\tau_i} \frac{1}{\iiint r_p(r,z)s_i(r,z)d\upsilon}, \tag{2}$$

where T_{oc} is the cavity transmittance for the laser emission wavelengths, $L_i = 1 - T_{Lyot,i}^2$ is the round-trip loss, which is caused by the LF, L_{0i} is the cavity round trip passive loss, l_c is the length of the Nd:LGAG, $\eta_{q',i}$ is the quantum efficiency, $h\nu_p$ is the photon energy of the pump beam, σ_i is the stimulated emission cross-section, τ_i is the upper energy level lifetime, $r_p(r,z)$ is the pump beam distribution of the normalized intensity in the Nd:LGAG, and $s_i(r,z)$ is the cavity mode distribution of the normalized intensity for the emission wavelength. $r_p(r,z)$ and $s_i(r,z)$ can be written by [47], respectively,

$$r_p(r,z) = \frac{\alpha e^{-\alpha z}}{\pi\omega_p^2(z)\left(1 - e^{-\alpha z}\right)} \Theta\left(\omega_p^2(z) - r^2\right), \tag{3}$$

and

$$s_i(r,z) = \frac{2}{\pi\omega_{i0}^2 l_c} exp\left(\frac{2r^2}{\omega_{i0}^2}\right), \tag{4}$$

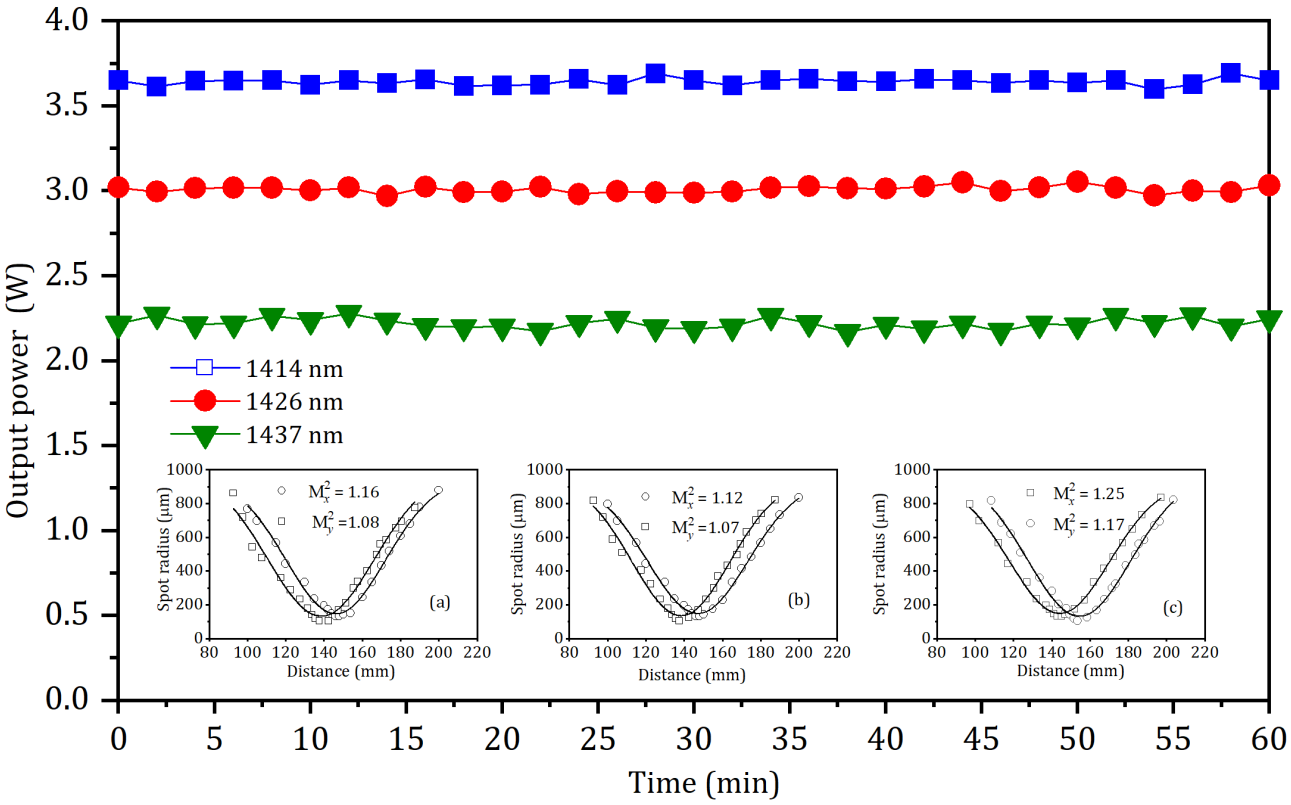

Fig 6. Power stabilities of the three laser wavelengths. Insets (a), (b) and (c) show the X- and Y-axes radii as functions of Z-axis position for the 1414 nm, 1426 nm and 1437 nm beams, respectively.

https://doi.org/10.1371/journal.pone.0333387.g006

where α is the absorption coefficient, $\Theta$is the Heaviside step function, ω_{0i} is the radius of the laser spot, and the size of the pump beam in the Nd:LGAG given by

$$\omega_p^2(z) = \omega_{p0}^2 \left\{ 1 + \left[\frac{\lambda_p M_p^2}{n\pi\omega_{p0}^2} (z - z_0) \right]^2 \right\}, \tag{5}$$

where ω_{p0} is the radius of the pump spot, λ_p is the pump wavelength, $M2$ $p$is the quality factor of the pump beam. With Eqs. (1)-(5) and the parameters in our experiment: T_{oc} = 3.5%, $\sigma_1 = 1.04 \times 10^{-20}$ cm^2, $\sigma_2 = 0.84 \times 10^{-20}$ cm^2, $\sigma_3 = 0.98 \times 10^{-20}$ cm^2, α = 3.5 cm^{-1}, l_c = 5 mm, ω_p = 200 μm, ω_{0i} = 190 μm, n = 1.83, M^2 = 3.5,$\eta_{q,i} \approx 0.57$, $\tau_i \approx 262$μs, $h\nu_p = 2.45 \times 10^{-19}$J, and L_{0i}=0.5% was measured using the Findlay-Clay method [48], the threshold was calculated as a function of tuning angle α for the three laser wavelengths, as displayed in Fig 7. It can be seen that the threshold can be controlled by regulating the LF. It can be observed that intersecting points exist between any two threshold power curves, indicating that the pump power required for lasing threshold is identical for both wavelengths at these intersection points. Consequently, DW lasers could be achieved when the pump powers were precisely regulated to these power levels.

When α was regulated to about 3.5°, 5.5°, and 16.5°, the three pairs of the DWs at 1414 nm and 1426 nm, 1414 nm and 1437 nm, and 1426 nm and 1437 nm were generated, respectively, and their output-input performances were displayed in Fig 8. At an absorbed power of 18.7 W, the total powers were 2.82 W (1.44 W at 1437 nm and 1.38 W at 1414 nm), 2.75

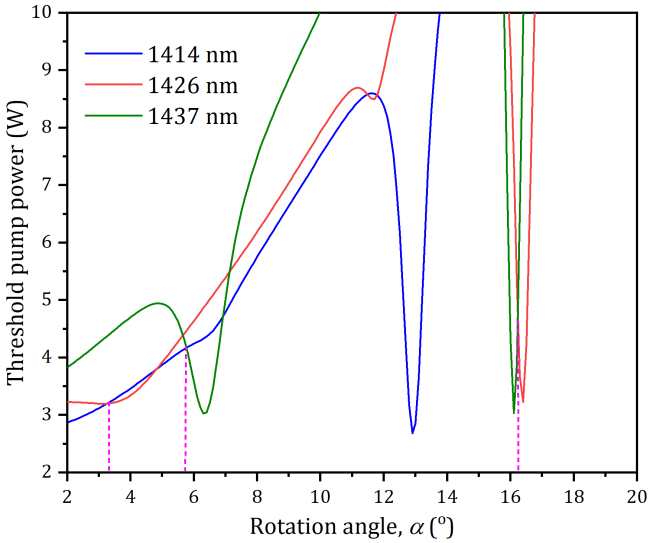

Fig 7. Tuning angle versus the threshold power.

https://doi.org/10.1371/journal.pone.0333387.g007

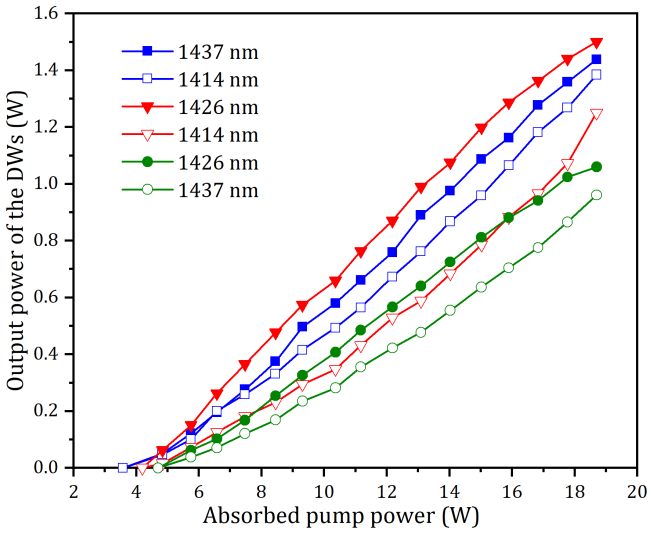

Fig 8. Output powers of DWs versus absorbed pump power.

https://doi.org/10.1371/journal.pone.0333387.g008

W (1.50 W at 1426 nm and 1.25 W at 1414 nm) and 2.12 W (1.06 W at 1426 nm and 0.96 W at 1437 nm) for the three pairs of DWs, respectively. The corresponding threshold powers were 3.58 W, 4.21 W and 4.72 W, respectively. The total optical conversion efficiencies with respect to the absorbed power were 15.1%, 14.7% and 11.3%, respectively. The laser spectra of the three pairs of DWs were displayed in the Fig 9. The corresponding peak wavelengths were 1413.83 nm and 1426.41 nm, 1413.95 nm and 1437.04 nm, 1426.44 nm and 1437.02 nm, respectively. For the three pairs of DWs, Their corresponding M^2 factors were 1.12 and 1.15, 1.18 and 1.24 and 1.22 and 1.27, respectively, and their power stabilities were about 2.5% and 2.9%, 2.8% and 3.8%, and 3.5% and 4.2%, respectively.

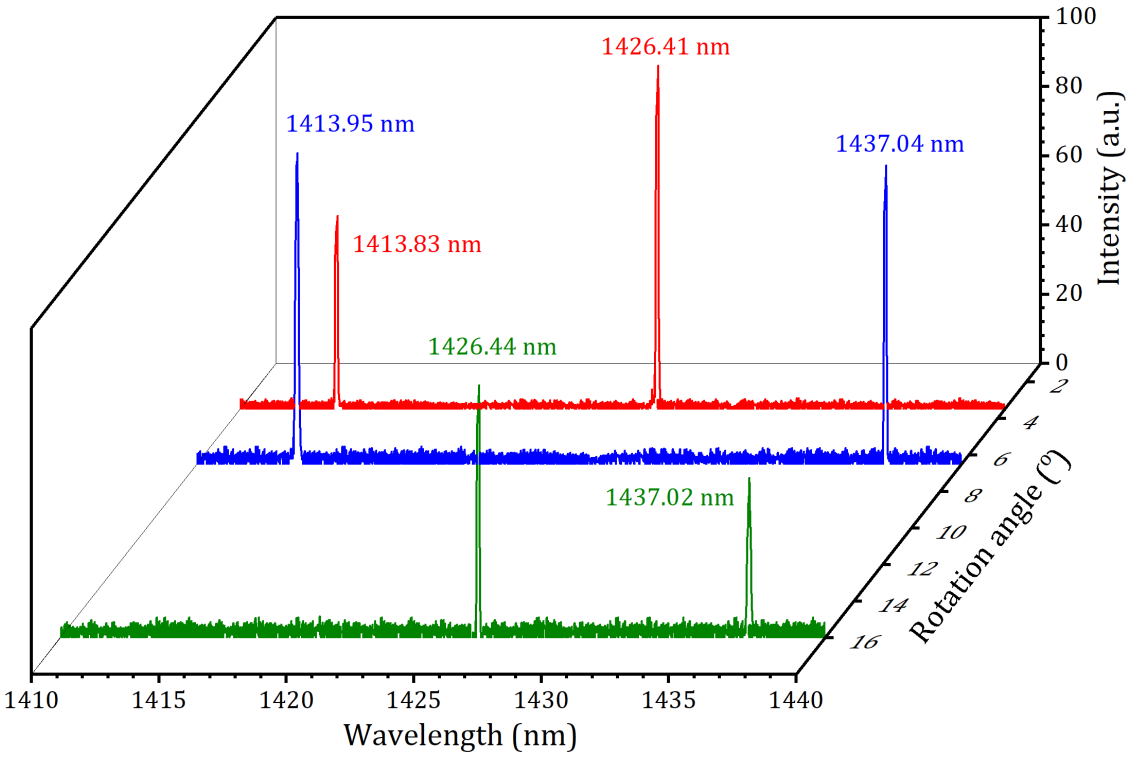

Fig 9. Laser spectra of the three pairs of DWs.

https://doi.org/10.1371/journal.pone.0333387.g009

Compared with the previously reported the 1.4 μm single-wavelength laser on Nd:GSAG crystal (slope efficiency of 13.6%, optical conversion efficiency of 11.5% [15]), the single-wavelength system in this study achieved a slope efficiency of 23.7% and an optical conversion efficiency of 19.5%. In terms of DW laser output, the total optical conversion efficiency has increased from 9.2% to 15.1%. These data fully demonstrate the significant progress of this laser system in the optical conversion efficiency at the 1.4 μm spectral region.

4. Conclusion

In conclusion, diode-pumped tunable single- and DW laser operation near 1.4 μm spectral region in Nd:LGAG on the $^4F_{3/2} \rightarrow {}^4I_{13/2}$ transition was demonstrated for the first time. By regulated an intracavity LF, the three single-wavelengths at 1414 nm, 1426 nm and 1437 nm were obtained, respectively. The maximum CWoutput power of 3.64 W at 1414 nm was attained under an absorbed pump power of 18.7 W, exhibiting a slope efficiency of 23.7% and optical conversion efficiency of 19.5%. Further, three pairs of DW lasers operating at 1414 nm and 1426 nm, 1414 nm and 1437 nm, and 1426 nm and 1437 nm were also achieved, respectively. The DW operation at 1414 nm and 1437 nm yielded 2.82 W total CW output power, attaining 15.1% total optical conversion efficiency. This study proposes a new method for generating tunable single- and DW lasers, which can be applied to other active medium to achieve laser output of different spectral regions.

Author contributions

Data curation: Haotian Huang, Yuzhao Li, Nguyen Tuan Anh, Jing Xia.

Formal analysis: Yuzhao Li.

Investigation: Yuzhao Li, Nguyen Tuan Anh.

Project administration: Yanfei Lü, Jing Xia.

Writing – original draft: Haotian Huang, Yuzhao Li, Yanfei Lü, Jing Xia.

Writing – review & editing: Yanfei Lü, Jing Xia.

References

1. Yu H, Li Y, Moazzam F, Lin L, Gao B. Orthogonally polarized dual-wavelength Nd:GdVO4/Nd:YVO4 laser at 1341 and 1342 nm with adjustable power ratio. PLoS ONE. 2025;20:e0317875.
2. Lü 2, Zhang J, Xia J, Liu H. Diode-Pumped Quasi-Three-Level Nd:YVO4 Laser with Orthogonally Polarized Emission. IEEE Photon Technol Lett. 2014;26:656–9.
3. Lü Y, Zhao L, Zhai P, Xia J, Fu X, and Li S. Simultaneous three-wavelength continuous-wave laser at 946 nm, 1319 nm and 1064 nm in Nd:YAG. Opt. Commun. 2013; 286: 257–60.
4. Lü Y, Xia J, Cheng W, Chen J, Ning G, Liang Z. Diode-pumped cw Nd:YAG three-level laser at 869 nm. Opt Lett. 2010;35(21):3670–2. https://doi.org/10.1364/OL.35.003670 PMID: 21042386
5. Czeranowsky C, Heumann E, Huber G. All-solid-state continuous-wave frequency-doubled Nd:YAG-BiBO laser with 2.8-W output power at 473 nm. Opt Lett. 2003;28(6):432–4. https://doi.org/10.1364/ol.28.000432 PMID: 12659270
6. Wu B, Jiang P, Yang D, Chen T, Kong J, Shen Y. Compact dual-wavelength Nd:GdVO4 laser working at 1063 and 1065 nm. Optics Express. 2009;17:6004–9.
7. Czeranowsky C, Schmidt M, Heumann E, Huber G, Kutovoi S, Zavartsev Y. Continuous wave diode pumped intracavity doubled Nd:GdVO4 laser with 840 mW output power at 456 nm. Opt Commun. 2002;205:361–5.
8. Pollak T, Wing W, Grasso R, Chicklis E, Jenssen H. CW Laser Operation of Nd:YLF. IEEE J Quantum Electron. 1982;18:159–63.
9. Xu S, Gao S. A new wavelength laser at 1370 nm generated by Nd:YLF crystal. Mater Lett. 2016;183:451–3.
10. Tzeng YS, Huang YJ, Tang CY, Su KW, Chen WD, Zhang G, et al. High-power tunable single- and multi-wavelength diode-pumped Nd:YAP laser in the (4)F3/2 → (4)I11/2 transition. Opt Express. 2013;21(22):26261–8. https://doi.org/10.1364/OE.21.026261 PMID: 24216850
11. Boucher M, Musset O, Boquillon J, Georgiou E. Multiwatt CW diode end-pumped Nd:YAP laser at 1.08 and 1.34 μm: influence of Nd doping level. Opt Commun. 2002;212:139–48.
12. Akbari R, Loiko P, Xu J, Xu X, Major A. Dual-wavelength Nd:CALGO laser based on differential loss of birefringent filter. Laser Phys Lett. 2024;21:015001.
13. Kallmeyer F, Dziedzina M, Wang X, Eichler H, Czeranowsky C, Ileri B, et al. Nd:GSAG-pulsed laser operation at 943 nm and crystal growth. Appl Phys B. 2007;89:305–10.
14. Wang X, Kallmeyer F, Chen J, Eichler H. Model of pulsed Nd:GSAG laser at 942 nm considering rate equations with cavity structure. Appl Phys B. 2008;92:43–8.
15. Chu C, Fu X, Li Y. Diode-pumped continuous-wave Nd:GSAG lasers operating at 1.4 μm. Opt Laser Technol. 2025;181:111846.
16. Lee H, Kima Y. Output characteristics of a flashlamp pumped Nd:YAG laser at 1444 nm. Opt Laser Technol. 2008;40:901–5.
17. Podlipensky A, Yumashev K, Kuleshov N, Kretschmann H, Huber G. Passive Q-switching of 1.44 lm and 1.34 lm diode-pumped Nd:YAG lasers with a V:YAG saturable absorber. Appl Phys B. 2003;76:245.
18. Šulc J, Novák J, Jelínková H, Nejezchleb K, Škoda V. 1444-nm Q-switched pulse generator based on Nd:YAG/V:YAG microchip laser. Laser Phys. 2010;20:1288.
19. Hodgson N, Nighan WL Jr, Golding DJ, Eisel D. Efficient 100-W Nd:YAG laser operating at a wavelength of 1.444 microm. Opt Lett. 1994;19(17):1328–30. https://doi.org/10.1364/ol.19.001328 PMID: 19855510
20. Liang W, Zhang X, Xia J, Jin G, Xu L, Sun G, et al. Diode-pumped continuous-wave eye-safe Nd:YAP laser at 1.43 μm. Laser Phys Lett. 2011;8:286.
21. Tark KC, Jung JE, Song SY. Superior lipolytic effect of the 1,444 nm Nd:YAG laser: comparison with the 1,064 nm Nd:YAG laser. Lasers Surg Med. 2009;41(10):721–7. https://doi.org/10.1002/lsm.20786 PMID: 20014250
22. Han S, Zhou Y, Wang Z, Hu D, Xu X, Yu H, et al. Graphene Q-switched 1.4 μm solid state laser. Laser Phys Lett. 2018;15:075801.
23. Tanzi EL, Alster TS. Comparison of a 1450-nm diode laser and a 1320-nm Nd:YAG laser in the treatment of atrophic facial scars: a prospective clinical and histologic study. Dermatol Surg. 2004;30(2 Pt 1):152–7. https://doi.org/10.1111/j.1524-4725.2004.30078.x PMID: 14756642
24. Perez-Maldonado A, Rünger TM, Krejci-Papa N. The 1,450-nm diode laser reduces sebum production in facial skin: a possible mode of action of its effectiveness for the treatment of acne vulgaris. Lasers Surg Med. 2007;39(2):189–92. https://doi.org/10.1002/lsm.20465 PMID: 17311272

25. Sabella A, Piper JA, Mildren RP. Efficient conversion of a 1.064 μm Nd:YAG laser to the eye-safe region using a diamond Raman laser. Opt Express. 2011;19(23):23554–60. https://doi.org/10.1364/OE.19.023554 PMID: 22109234
26. Kubo T, Kane T. Diode-pumped lasers at five eye-safe wavelengths. IEEE J Quantum Electron. 1992;28:1033–40.
27. Mackenzie J, Szela J, Beecher S, Parsonage T, Eason R, Shepherd D. Crystal planar waveguides, a power scaling architecture for low-gain transitions. IEEE J Sel Topics Quantum Electron. 2015;21:380–9.
28. Di J, Xu X, Xia C, Tan W, Zhang J, Tang D, et al. Highly efficient passive mode locking of Nd:Lu2.9Gd0.1Al5O12 garnet crystal. Laser Phys. 2013;23:055803.
29. Zhuang S, Han S, Wang Z, Hu D, Xu X, Yu H. Efficient quasi-three-level laser operation of Nd:Gd:LuAG crystal and blue light generation. IEEE Photon Technol Lett. 2013;25:355–8.
30. Di J, Xu X, Cheng S, Li D, Zhou D, Wu F, et al. Crystal growth, spectroscopic and CW laser properties of Nd0.03Lu2.871Gd0.099Al5O12 crystal. Laser Phys. 2011;21:1891–4.
31. Huber G, Krühler W, Bludau W, Danielmeyer H. Anisotropy in the laser performance of NdP5O14. J Appl Phys. 1975;46:3580–4.
32. Farley RW, Dao PD. Development of an intracavity-summed multiple-wavelength Nd:YAG laser for a rugged, solid-state sodium lidar system. Appl Opt. 1995;34(21):4269–73. https://doi.org/10.1364/AO.34.004269 PMID: 21052256
33. Son SN, Song J-J, Kang JU, Kim C-S. Simultaneous second harmonic generation of multiple wavelength laser outputs for medical sensing. Sensors (Basel). 2011;11(6):6125–30. https://doi.org/10.3390/s110606125 PMID: 22163945
34. Weigl F. Two-wavelength holographic interferometry for transparent media using a diffraction grating. Appl Opt. 1971;10(5):1083–6. https://doi.org/10.1364/AO.10.001083 PMID: 20094606
35. Fu Q, Dong C, Wang K, He Q, Gu X, Liu J, et al. Underwater target laser polarization suppression scattering detection technology and verification. PLoS One. 2024;19(6):e0305929. https://doi.org/10.1371/journal.pone.0305929 PMID: 38917184
36. Basov N, Gubin M, Nikitin V, Nikuchin A, Petrovskii V, Protsenko E, et al. Highly-sensitive method of narrow spectral-line separations, based on the detection of frequency resonances of a 2-mode gas-laser with non-linear absorption. Izv Akad Nauk SSSR, Ser Fiz. 1982;46:1573–83.
37. Zhang S, Tan Y, Li Y. Orthogonally polarized dual frequency lasers and applications in self-sensing metrology. Meas Sci Technol. 2010;21:054016.
38. Fei L, Zhang S. The discovery of nanometer fringes in laser self-mixing interference. Optics Communications. 2007;273:226–30.
39. Daykin J, Woods JRC, Bek R, Jetter M, Michler P, Mills B, et al. Bi-frequency operation in a membrane external-cavity surface-emitting laser. PLoS One. 2023;18(7):e0289223. https://doi.org/10.1371/journal.pone.0289223 PMID: 37498940
40. Chen Y, Tsai S. Diode-pumped Q-switched laser with intracavity sum frequency mixing in periodically poled KTP. Appl Phys B. 2004;79:207–10.
41. Zhao P, Ragam S, Ding Y, Zotova I. Power scalability and frequency agility of compact terahertz source based on frequency mixing from solid-state lasers. Appl Phys Lett. 2011;98:131106.
42. Tanoto H, Teng J, Wu Q, Sun M, Chen Z, Maier S, et al. Greatly enhanced continuous-wave terahertz emission by nano-electrodes in photoconductive photomixer. Nature Photonics. 2012;6:121–6.
43. Bernenko D, Li M, Månefjord H, Jansson S, Runemark A, Kirkeby C, et al. Insect diversity estimation in polarimetric lidar. PLoS One. 2024;19(11):e0312770. https://doi.org/10.1371/journal.pone.0312770 PMID: 39485810
44. Sun T, Guo Y, Wang T, Huo J, Zhang L. Widely tunable wavelength spacing dual-wavelength single longitudinal mode erbium doped fiber laser. Opt Fiber Technol. 2014;20:235–8.
45. Huang H, Xia J, Anh N, Li Y, Lü Y. Dual-wavelength operation at 607 nm and 640 nm with the same threshold and slope efficiency in Pr3 :LiLuF4 crystal. Photonics. 2025;12:447.
46. Fan T, Byer R. Diode laser-pumped solid-state lasers. IEEE J Quantum Electron. 1988;24:895.
47. Chen Y. cw dual-wavelength operation of a diode-pumped Nd:YVO4 laser. Appl Phys B. 2000;70:475–8.
48. Findlay D, Clay R. The measurement of internal losses in 4-level lasers. Phys Lett. 1966;20:277–8.